Progress In Electromagnetics Research, PIER 66, 239–251, 2006

PLANAR METAMATERIALS SUPPORTING MULTIPLE LEFT-HANDED MODES

Y. Guo and R. Xu

School of Electronic Engineering
University of Electronic Science and Technology of China
Chengdu, Sichuan 610054, P. R. China

Abstract—Planar metamaterials with spiral elements are suggested in this paper to support multiple left-handed (LH) modes. Compared with previously proposed split-loop metamaterial, spiral arrays are found to support hybrid TE and TM LH modes. Dispersion diagrams and field distributions are carried out to demonstrate the existence of the hybrid LH modes. Array with double-spiral elements can be viewed as a spiral split-loop array, which leads a very interesting dual-LH-band feature. It can be explained as a combination of spiral and split-ring arrays has similar mechanism with the multiband frequency selective surfaces (FSS), which have multiple resonators in a single unit cell. The two LH modes are TE and TM modes respectively. Validations of the multiple LH modes are presented by means of full-wave simulation using commercial software (Ansoft HFSS).

1. INTRODUCTION

Metamaterials, which are materials with simultaneously negative permittivity (ε) and permeability (μ), were first theorized by Veselago in 1968 [1]. They are also known as left-handed (LH) materials because of the fact that the vectors $\boldsymbol{E}$, $\boldsymbol{H}$ and $\boldsymbol{k}$ form a left-handed triplet, instead of a right-handed (RH) triplet in conventional media. In LH media the Poynting vector $\boldsymbol{E} \times \boldsymbol{H}$ (that points at the direction of energy propagation and the group velocity) is anti-parallel to the wave vector $\boldsymbol{k}$ (that points at the direction of phase velocity). As a result, unique electromagnetic properties, such as backward-wave propagation and negative refractive index, can be observed from these materials. Recently, artificial structures with negative ε and negative μ have been synthesized using thin wires and split-ring resonators (SRR) [2, 3]. A transmission-line approach for the analysis and design of

planar LH media was carried out by different researchers at almost the same time [4–6]. Based on this approach, distributed planar LH structures have also been presented [7, 8]. Applications of the planar LH structures to microwave components have been proposed such as antenna [9, 10, 24], phase shifter [11–13], coupler [14, 15], balun [16] and power divider [17]. More recently, three-dimensional metamaterials [25] and matamaterials in terahertz [26] have been reported as well.

Uniplanar designs have been presented in [18] and [19] with anisotropic split-loop element and isotropic spiral element. Compared with those in [7] and [8], these designs are completely planar without any shunt vias or vertical insertions through the dielectric substrates. Fundamental TE LH modes are found to be supported by these arrays unlike the TM LH modes in the previous two-dimensional designs in [7] and [8]. A more complex geometry of double-spiral element, which shows a similar left-handedness with the split-loop element, was also mentioned in [19] as a compact design.

Further study of the uniplanar structures is carried out in this paper. Dispersion diagrams are presented to locate the LH modes. Field distributions are then given out to identify the polarizations of the electric and magnetic fields associated with these LH modes. Split-loop array, as it is expected in [18] and [19], has a TE-dominant field polarization for LH propagation. A single LH mode is found from the dispersion diagram of spiral array. However, hybrid TE and TM polarizations can be observed from the field distributions. To confirm it is a hybrid mode, slight change is applied to the layout of the spiral array. As a result, the hybrid property is clearly demonstrated by its dispersion characteristic. It is interesting to find that double-spiral array has a more unique feature of dual LH bands. These two LH modes are predominant TE and TM respectively. According to the surface-current distribution analysis, it can be explained as that the double-spiral element acts like multiple resonator combined by the split-ring and spiral geometries, which contribute to these two different LH modes.

In the following sections of this paper, full-wave simulations of finite spiral and double-spiral array are presented by using commercial software (Ansoft HFSS). TE and TM surface-wave propagations are validated with TE and TM excitations. Another simulation of a microstrip transmission line with double-spiral array as substrate is also presented to demonstrate the multiple LH pass-bands of the double-spiral array. Measurement of a finite spiral array with microstrip-line feedings is carried out to prove the negative phase velocity of the LH propagation.

2. ANALYSIS

2.1. Split-loop Array

All the arrays discussed hereafter are metallic lines printed on the grounded dielectric substrates with a dielectric constant of 2.2 and thickness 1.13 mm. The unit element of the split-loop array is shown in Fig. 1 as the inset. The size of the unit cell is (3 mm×6 mm). The element dimension is (2.8 mm×5.8 mm).The metallic line, as well as the gap, is 0.2 mm wide.

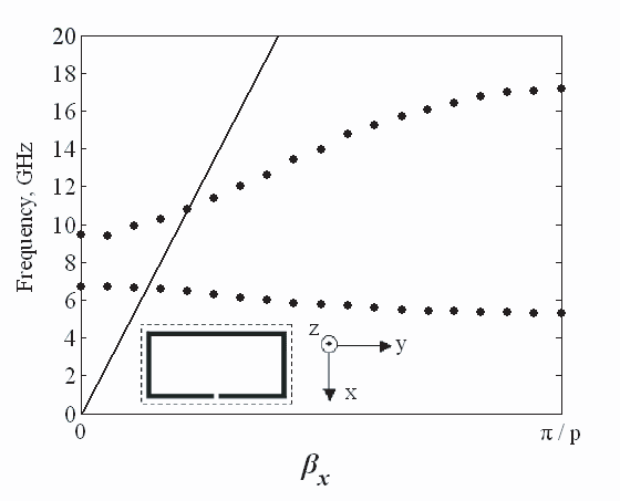

Figure 1. Dispersion diagram of split-loop array. Unit element of the array is shown as the inset.

The dispersion diagram is presented in Fig. 1. Because the propagation characteristics of the arrays we study throughout this paper are all along x-direction, only $f - \boldsymbol{\beta_x}$ part of the dispersion diagram is given here. The range of $\boldsymbol{\beta_x}$ varies from 0 to π/p, where p is the periodicity of the array in x-direction. The curves formed by the dots stand for the propagation modes. The first resonant mode (5.3 GHz to 6.7 GHz) indicates the array as a LH medium within this frequency range because of the negative gradient of the dispersion curve, which corresponds to the anti-parallel fact of the phase velocity (ω/β) and the group velocity ($d\omega/d\beta$). Contrarily, the second resonant mode (9.4 GHz to 17.2 GHz) is a right-handed (RH) mode. The split-loop array in this range works as a normal electromagnetic band-gap (EBG) material for the positive phase velocity of supported waves. A light line is also included in this dispersion diagram.

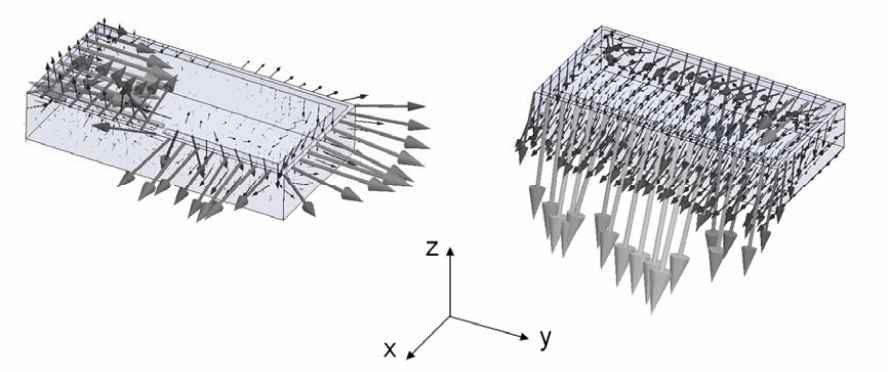

Figure 2. Filed distributions in the unit cell of split-loop array at 6 GHz. (a) Electric field distribution. (b) Magnetic field distribution.

Field distribution in the unit cell is shown in Fig. 2 to check the field polarization of the LH mode. Frequency is set to be 6 GHz which is within the LH range. The electric field polarization is basically parallel to x-direction while the magnetic field polarization lies in the x-z plane. Therefore, in the x-direction the first resonant mode is predominantly TE.

2.2. Spiral Array

A spiral design is shown in Fig. 3. Arrays with this type of elements are demonstrated to be isotropic, which have the same dispersion curves in x- and y-directions. The design in Fig. 3 has a unit-cell size of (3 mm×3 mm). The element dimension is (2.8 mm×2.8 mm), which is half of that in the split-loop array. The metallic line width is 0.2 mm. The gap coiled inside the element is 0.4 mm wide.

The $f-\boldsymbol{\beta}_{\boldsymbol{x}}$ dispersion diagram is shown in Fig. 3. Similar situation with that of the split-loop array is found as a first resonant LH mode (6.3 GHz to 7.6 GHz) and a second resonant RH mode (11.1 GHz to 15.2 GHz). However, the field distribution in this case is quite different with that of the split-loop array. Choosing frequency point at 7 GHz, both TE and TM polarizations are observed as what is shown in Fig. 4. It suggests that this LH mode is a hybrid mode composed of two superposed TE and TM LH modes.

In order to confirm the guess above, we make some change to the array layout. Elements are flipped over around x-axis at intervals of one element along y-direction. Unit cell element in the new array becomes paired-spiral element as is inserted in Fig. 5. Because spirals are not axis-symmetric shapes, coupling along y-direction will

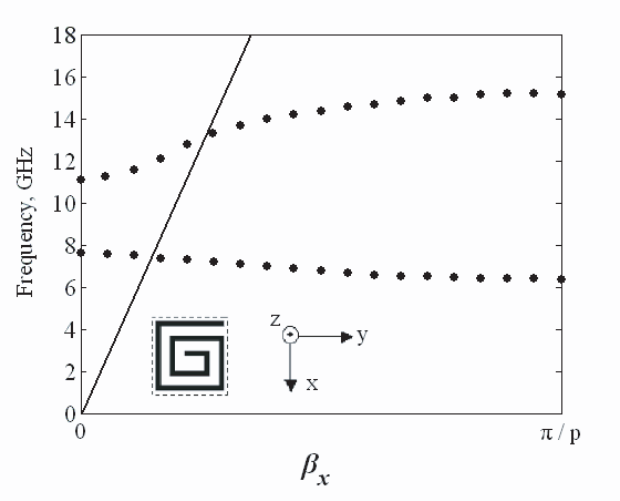

Figure 3. Dispersion diagram of spiral array. Unit element of the array is shown as the inset.

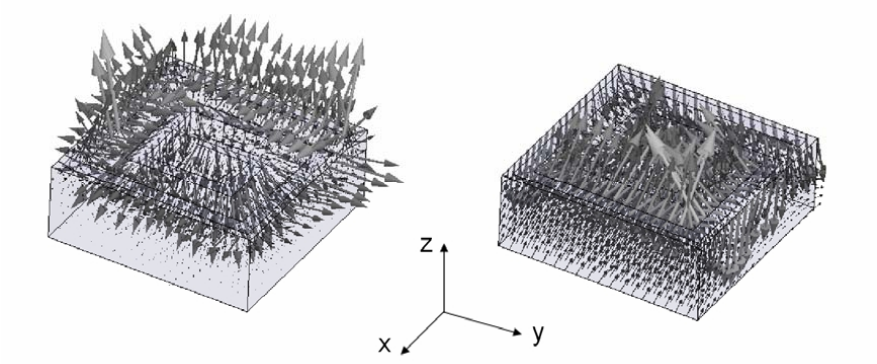

Figure 4. Filed distributions in the unit cell of spiral array at 7 GHz. (a) Electric field distribution. (b) Magnetic field distribution.

vary from that along x-direction after the elements are overturned. Dispersion diagram of the paired-spiral array is derived as Fig. 5 shows. The hybrid LH modes are clearly presented. It is worth noting that not only the fundamental LH modes but also the RH modes at higher frequency range are hybrid TE and TM modes. This unique feature is contributed by the quasi-central-symmetric property of spiral shape.

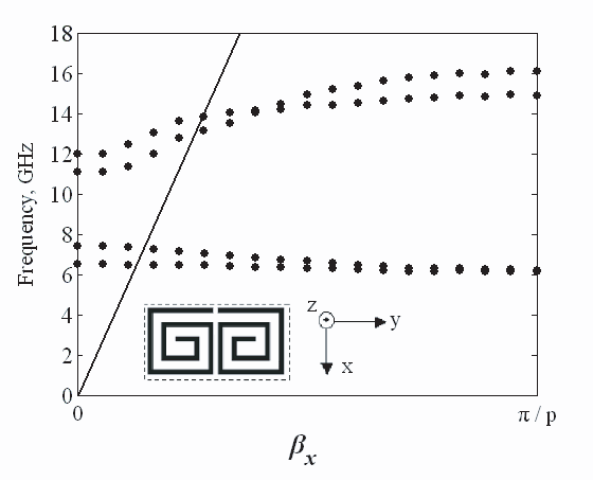

Figure 5. Dispersion diagram of paired-spiral array. Unit element of the array is shown as the inset.

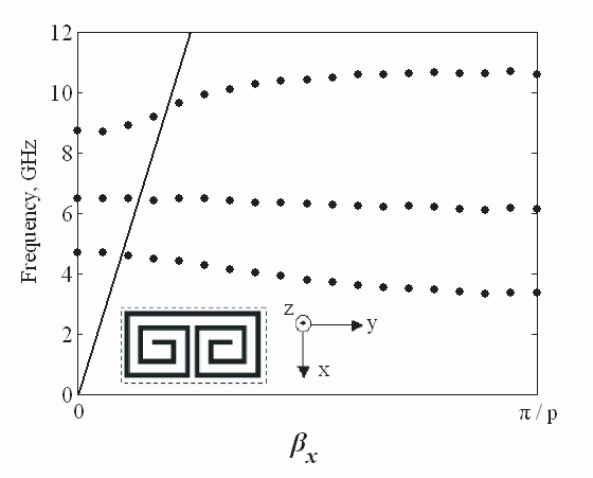

Figure 6. Dispersion diagram of double-spiral array. Unit element of the array is shown as the inset.

2.3. Double-spiral Array

By simply connected of the ends facing together, the two counterparts of the paired-spiral elements in Fig. 5 form the double-spiral element as is shown in Fig. 6. Array with this element has been previously introduced in [19] as a compact design of uniplanar metamaterial which works at a very low frequency of 3.3 ghz to 4.7 ghz. Only fundamental

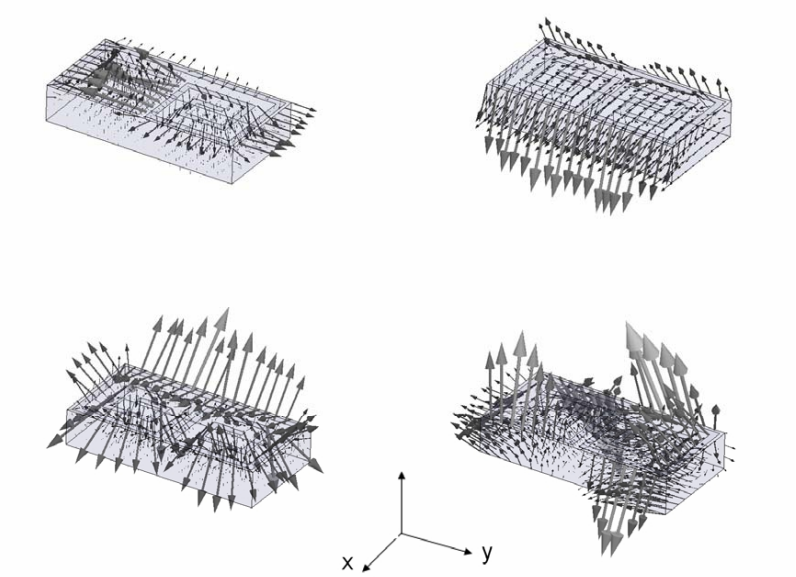

Figure 7. Filed distributions in the unit cell of double-spiral array. (a) Electric field distribution at 4 GHz. (b) Magnetic field distribution at 4 GHz. (c) Electric field distribution at 6.3 GHz. (b) Magnetic field distribution at 6.3 GHz.

LH mode was studied in [19] to show the miniaturization. Dispersion diagram for a larger frequency range is produced in Fig. 6. It is interesting to find that the second resonant mode (6.1 GHz to 6.5 GHz) is a LH mode again. Bandwidth of this LH mode is much narrower than that of the fundamental LH mode. A RH mode is also found at higher frequency range (8.7 GHz to 10.6 GHz).

Surface current distributions at resonant frequencies over the elements of the double spiral array, as well as the split-loop array and the spiral array are carried out in Fig. 8 to study this multi-band LH property. Similar with the multi-band frequency selective surfaces (FSS) with multi-resonator unit-cell elements [20–22], the double-spiral array is considered as a combo of a split-loop array and a spiral array. Surface current distributions over the double-spiral element at 4 GHz and 6.3 GHz, which are associated to the first and the second LH modes respectively, are shown as Fig. 8(c) and Fig. 8(d). Surface current distributions over the split-loop element at 6 GHz and over the spiral element at 7 GHz are also presented in Fig. 8(a) and Fig. 8(b) as comparisons. Fig. 8 shows that the double-spiral array works like the split-loop array in Fig. 1 for first LH mode and like the paired-spiral

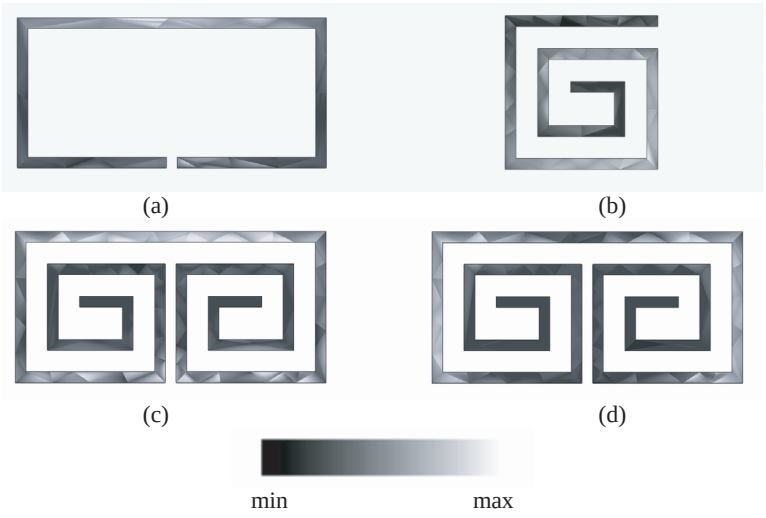

Figure 8. Surface current distributions over the array elements. (a) Split-loop element at 6 GHz. (b) Spiral element at 7 GHz. (c) Double-spiral element at 4 GHz. (b) Split-loop element at 6.3 GHz.

array in Fig. 5 for second LH mode. The corresponding LH frequency bands of the double-spiral array are lower than those of the split-loop array and spiral array. This is caused by the longer electrical length of the double-spiral element.

3. SIMULATION

3.1. Metamaterial Substrates

Full-wave simulation of a transmission-line structure is presented to demonstrate the band-pass property of the double-spiral array in Fig. 6 using commercial software (Ansoft HFSS) [23]. Two rows of the double-spiral array mentioned in the previous section are used in the simulation as part of the substrate. An overhead microstrip transmission line along x-direction is put above the array. The dielectric layer between the microstrip line and the array surface is 0.07mm thick with a dielectric constant of 2.2. Because microstrip lines support quasi-TEM wave, both TE and TM modes can be excited in this model.

Simulated result is shown in Fig. 9. Two different LH bands and a RH band are all presented as what the dispersion diagram predicted. The pass-bands of the double-spiral array in derived in the simulation

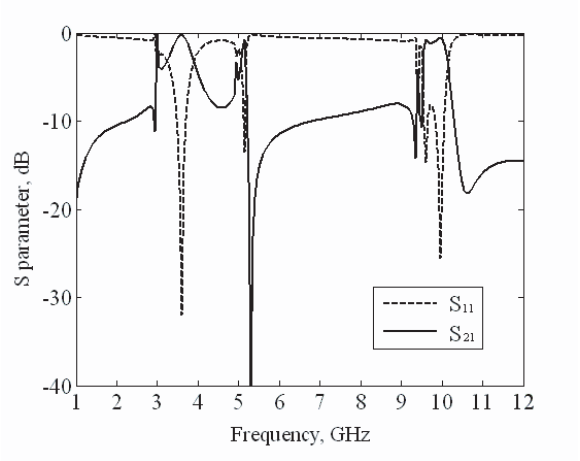

Figure 9. Simulated S parameter of microstrip transmission line with two rows of double-spiral array as substrate.

with center frequencies of 3.6 GHz, 5 GHz and 9.7 GHz. Compared with the dispersion diagram in Fig. 6, the LH modes are observably affected by the added microstrip transmission line. There are frequency offsets of about 10% and 20% to lower region for the first and second LH modes separately, while the resonant frequency of the RH mode has a good agreement to the dispersion prediction.

3.2. Validation of TE and TM Propagations

In order to validate the TE and TM propagations of the LH modes, finite structures of paired-spiral element in Fig. 5 and double-spiral element in Fig. 6 is simulated, which are similar with the model of the loaded split-loop array in [19]. Four elements are placed in x-dimension with a perfect electric conductor (PEC) boundary condition assigned on either side. Waveguide excitations with TE and TM polarizations are applied. Transmission coefficients are derived as Fig. 10 shows. In Fig. 10(a), the bold curve stands for the TE response of the paired-spiral array (6.1 GHz to 7.2 GHz) which has a wider frequency range than the TM response (6.1 GHz to 6.5 GHz) as the dispersion diagram in Fig. 5 predicts. In Fig. 10(b), the ranges of the TE pass-band are (3.3 GHz to 4.5 GHz) and (9.2 GHz to 10.6 GHz) corresponding to the first LH mode and the RH mode. With TM polarization, only s single pass-band of (6.1 GHz to 6.4 GHz) is shown as the dash curve. Because only the dispersion curves at right side of the light line in the dispersion diagram indicate the bounded-wave modes, the simulated result is in very good agreement to what is predicted in Fig. 5 and Fig. 6.

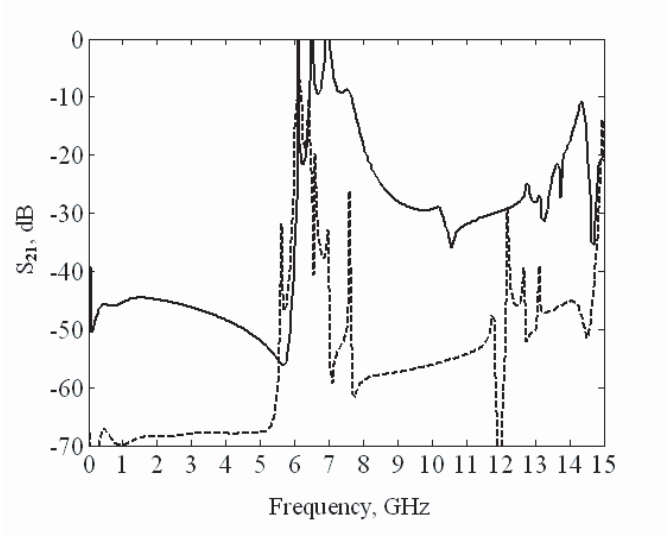

(a)

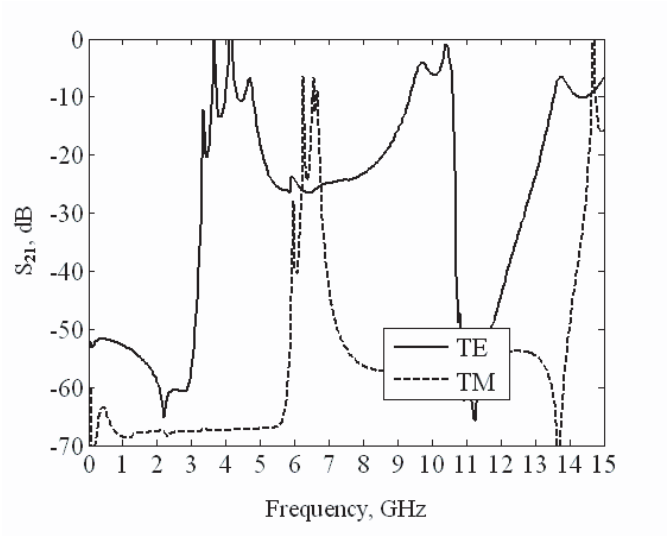

(b)

Figure 10. Simulated TE and TM transmission response of the finite structures. (a) Paired-spiral array in Fig. 5. (b) Double-spiral array in Fig. 6.

4. CONCLUSION

In this paper, planar metamaterials with spiral-based elements have been demonstrated to support multiple left-handed (LH) modes. Hybrid and separate TE and TM LH surface-wave modes are found in spiral array and double-spiral array respectively. Dispersion diagrams and field distributions have been presented to identify these modes. Multi-band property of the double-spiral array is theoretically explained and validated by the full-wave simulation using commercial software (Ansoft HFSS). TE and TM polarizations of the LH modes in these spiral-based structures are also demonstrated in simulations. These unique characteristics of these spiral-based arrays can be used to implement the isotropic, multi-band and broadband features in antenna and microwave circuit designs.

REFERENCES

1. Veselago, V. G., "The electrodynamics of substances with simultaneously negative values of ε and μ," *Sov. Phys. Usp.*, Vol. 10, No. 4, 509–514, Jan.–Feb. 1968.
2. Pendry, J. B., A. J. Holden, D. J. Robbins, and W. J. Stewart, "Magnetism from conductors and enhanced nonlinear phenomena," *IEEE Trans. Microwave Theory Tech.*, Vol. 47, No. 11, 2075–2084, Nov. 1999.
3. Smith, D. R., W. J. Padilla, D. C. Vier, S. C. Nemat-Nasser, and S. Schultz, "A composite medium with simultaneously negative permeability and permittivity," *Phys. Rev. Lett.*, Vol. 84, No. 18, 4184–4187, May 2000.
4. Eleftheriades, G. V., A. Iyer, and P. Kremer, "Planar negative refractive index media using periodically L-C loaded transmission lines," *IEEE Trans. Microwave Theory Tech.*, Vol. 50, No. 12, 2702–2711, Dec. 2002.
5. Caloz, C., H. Okabe, I. Awai, and T. Itoh, "Transmission line approach of left-handed materials," *IEEE AP-S USNC/URSI National Radio Science Meeting Digest*, 39, June 2002.
6. Oliner, "A periodic structure negative refractive index medium without resonant elements," *IEEE AP-S USNC/URSI National Radio Science Meeting Digest*, 41, June 2002.
7. Grbic, and G. V. Eleftheriades, "Periodic analysis of a 2-D negative refractive index transmission line structure," *IEEE Trans. Antennas and Propag.*, Vol. 51, No. 10, 2604–2611, Oct. 2003.

8. Sanada, A., C. Caloz, and T. Itoh, "Planar distributed structures with negative refractive index," *IEEE Trans. Microwave Theory Tech.*, Vol. 52, No. 4, 1252–1263, Apr. 2004.
9. Sanada, A., M. Kimura, I. Awai, H. Kubo, C. Caloz, and T. Itoh, "A planar zeroth order resonator antenna using left-handed transmission line," *European Microwave Conference Digest*, Vol. 2, 1341–1344, Oct. 2004.
10. Lim, S., C. Caloz, and T. Itoh, "Metamaterial-based electronically controlled transmission-line structure as a novel leaky-wave antenna with tunable radiation angle and beamwidth," *IEEE Trans. Microwave Theory Tech.*, Vol. 53, No. 1, 161–173, Jan. 2005.
11. Antoniades, M. A. and G. V. Eleftheriades, "Compact linear lead/lag metamaterial phase shifters for broadband applications," *IEEE Antennas Wireless Propag. Lett.*, Vol. 2, 103–106, 2003.
12. Islam, R., F. Elek, and G. V. Eleftheriades, "Coupled-line metamaterial coupler having co-directional phase but contra-directional power flow," *Electronic Letters*, Vol. 40, No. 5, 315–317, Mar. 2004.
13. Kim, H., A. B. Kozyrev, A. Karbassi, and D. W. van der Weide, "Linear tunable phase shifter using a left-handed transmission line," *IEEE Microwave and Wireless Components Letters*, Vol. 15, No. 5, 366–368, 2005.
14. Islam, R. and G. V. Eleftheriades, "Phase-agile branch-line couplers using metamaterial lines," *IEEE Microwave and Wireless Components Letters*, Vol. 14, 340–342, 2004.
15. Caloz, C., A. Sanada, and T. Itoh, "A novel composite right-/left-handed coupled-line directional coupler with arbitrary coupling level and broad bandwidth," *IEEE Trans. Microwave Theory and Techniques*, Vol. 52, No. 3, 980–992, Mar. 2004.
16. Antoniades, M. A. and G. V. Eleftheriades, "A broadband Wilkinson balun using microstrip metamaterial lines," *IEEE Antennas Wireless Propag. Lett.*, Vol. 4, 209–212, 2005.
17. Antoniades, M. A. and G. V. Eleftheriades, "A broadband series power divider using zero-degree metamaterial phase-shifting lines," *IEEE Microwave and Wireless Components Letters*, Vol. 15, No. 11, 808–810, 2005.
18. Goussetis, G., A. P. Feresidis, S. Wang, Y. Guo, and J. C. Vardaxoglou, "Planar left-handed artificial metamaterials," *J. Opt. A: Pure Appl. Opt.*, Vol. 7, No. 2, S44–S50, Feb. 2005.
19. Guo, Y., G. Goussetis, A. P. Feresidis, and J. C. Vardaxoglou,

"Efficient modeling of novel uniplanar left-handed metamaterials," *IEEE Transactions on Microwave Theory and Techniques*, Vol. 53, No. 4, 1462–1468, Apr. 2005.

20. Hill, R. A. and B. A. Munk, "The effect of perturbating a frequency selective surface and its relation to the design of a dual-band surface," *IEEE Trans. Antennas Propagat.*, Vol. 44, 368–374, Mar. 1996.
21. Parker, E. A. and J. C. Vardaxoglou, "Plane-wave illumination of concentric-ring frequency-selective surfaces," *Proc. IEE - Microwaves, Opt., Antennas*, Pt. H, Vol. 132, No. 3, 176–180, June 1985.
22. Wu, T. K. and S. W. Lee, "Multiband frequency surface with multiring patch elements," *IEEE Trans. Antennas Propagat.*, Vol. 42, No. 11, 1484–1490, Nov. 1994.
23. High Frequency Structure Simulator (HFSS), ver. 9.0, Ansoft Corporation, 2003.
24. Wu, B.-I., W. Wang, J. Pacheco, X. Chen, T. M. Grzegorczyk, and J. A. Kong, "A study of using metamaterials as antenna substrate to enhance gain," *Progress In Electromagnetics Research*, PIER 51, 295–328, 2005.
25. Yao, H.-Y., L.-W. Li, Q. Wu, and J. A. Kong, "Macroscopic performance analysis of metamaterials synthesized from microscopic 2-D isotropic cross split-ring resonator array," *Progress In Electromagnetics Research*, PIER 51, 197–219, 2005.
26. Wongkasem, N., A. Akyurlu, J. Li, A. Tibolt, Z. Kang, and W. D. Goodhue, "Novel broadband terahertz negative refractive index metamaterials: Analysis and experiment," *Progress In Electromagnetics Research*, PIER 64, 205–218, 2006.